Mon. Not. R. Astron. Soc. **288,** 596–608 (1997)

Spectral effects of the vacuum resonance in soft gamma-ray repeaters

Tomasz Bulik[1,2] and M. Coleman Miller[1★]

[1] *University of Chicago, Department of Astronomy and Astrophysics, 5640 S. Ellis, Chicago, IL 60637, USA*
[2] *N. Copernicus Astronomical Center, Bartycka 18, PL-00-716, Warsaw, Poland*

Accepted 1997 February 10. Received 1996 March 25

ABSTRACT

The association of all three soft gamma-ray repeaters (SGRs) with supernova remnants has established that SGRs are young neutron stars, and has given us a starting point for detailed modelling. One of the most popular classes of models involves strongly magnetized neutron stars, with surface dipole fields $B \sim 10^{14}$–10^{15} G. In such strong magnetic fields, many otherwise negligible processes can play an important role. Here we consider the effects of vacuum polarization on Compton scattering. Vacuum polarization introduces a characteristic density-dependent photon frequency at which the normal modes of polarization become non-orthogonal and the mean free path of photons decreases sharply. Our analytic results and Monte Carlo simulations of photon propagation through a magnetized plasma show that this effect leads, under a wide range of physical conditions, to a broad absorption-like feature in the energy range $\sim$5–40 keV. We discuss this effect in light of the spectra from SGR 1806 − 20.

Key words: magnetic fields – radiative transfer – stars: neutron – gamma-rays: theory.

1 INTRODUCTION

The first soft gamma-ray repeater (SGR) to be discovered, SGR 0525 − 66 (Mazets & Golenetskii 1981; Mazets et al. 1979), was shown soon after its discovery to be positionally coincident with the N49 supernova remnant in the Large Magellanic Cloud (Evans et al. 1980). More recently, the other two SGRs (SGR 1806 − 20 and 1900 + 14) have also been associated with supernova remnants (Kouveliotou et al. 1993, 1994; Kulkarni & Frail 1993; Hurley et al. 1994; Kulkarni et al. 1994). These associations have led to a consensus that SGRs originate from young neutron stars.

The peak luminosities inferred for bursts from SGRs are typically 10^{40}–10^{42} erg s^{-1} for $\sim$0.1–1 s (excepting the unusual 1979 March 5 event from SGR 0525 − 66, which had an inferred peak luminosity of $\sim 2 \times 10^{45}$ erg s^{-1}). These luminosities are $\sim 10^{2}$–10^{4} times the Eddington luminosity $L_{\rm E} \equiv 1.3 \times 10^{38} (M/{\rm M}_{\odot})$ erg s^{-1} at which the radial radiation force from Thomson scattering exactly balances the gravitational force on a fully ionized hydrogen plasma. None the less, the spectrum from SGR 1806 − 20, which has undergone bursts more than 110 times and is thus the best-studied of the SGRs, appears not to undergo the reddening one would expect if the burst created an expanding optically thick fireball (Fenimore, Laros & Ulmer 1994). Thus, despite the highly super-Eddington luminosities, the plasma is probably confined near the surface of the neutron star. Magnetic fields could confine the plasma, and perhaps suppress plasma instabilities, with pulsar-like field strengths of $\sim 10^{12}$ G (Lamb 1982; Katz 1982, 1993, 1994).

There are lines of argument suggesting much greater field strengths, of the order of 10^{14}–10^{15} G. As suggested in Thompson & Duncan (1995), a $\sim 6 \times 10^{14}$ G field could, within the $\sim 10^{4}$-yr lifetime of the N49 supernova remnant, spin a neutron star down to the 8-s period seen in the March 5 event. Moreover, a superstrong magnetic field may be able to account for the energetics and time-scales of SGRs (see Thompson & Duncan 1995 for one model). These models are extremely complicated, and there are many aspects of microscopic physics that are important only in very strong magnetic fields. Here we concentrate on the effects of vacuum polarization and, in particular, on the spectral effects of the second vacuum frequency.

In strong magnetic fields $B \gtrsim B_{\rm c}$, where $B_{\rm c} \equiv m_{\rm e}^2 c^3 / \hbar e = 4.414 \times 10^{13}$ G is the magnetic field at which the electron cyclotron energy equals the electron rest mass energy, vacuum polarization from virtual e^+e^- pairs can become significant (see e.g. Mészáros 1992 for a discussion). In fact,

★ *Compton GRO* Fellow.

for strong enough fields the vacuum contribution to the dielectric tensor can exceed the plasma contribution (Pavlov & Shibanov 1979; Ventura, Nagel & Mészáros 1979; Pavlov & Gnedin 1984). This has effects on the normal modes and cross-sections for photons. Well below the electron cyclotron frequency $\omega_B \equiv eB/m_e c$, the polarization normal modes for photons in a very strong magnetic field are close to linear over most photon frequencies and incident angles.

At most photon frequencies $\omega \ll \omega_B$, the scattering cross-section depends strongly on the polarization of the photon. If the electric field vector of the photon is in the plane formed by the magnetic field and the photon propagation direction $\hat{\boldsymbol{k}}$, the photon is in the parallel mode and the scattering cross-section is $\sigma_1 \sim \sigma_T$, where $\sigma_T = 6.65 \times 10^{-25}$ cm^2 is the Thomson cross-section. If the electric field vector of the photon is perpendicular to the $\boldsymbol{B}$–$\hat{\boldsymbol{k}}$ plane, the photon is in the perpendicular mode and $\sigma_2 \sim (\omega/\omega_B)^2 \sigma_T \ll \sigma_T$; this reduction in cross-section is understandable, because in a strong magnetic field it is easier to oscillate an electron along the field than to oscillate it across the field.

There is, however, a small range of photon frequencies in which the vacuum and plasma contributions to the dielectric tensor are comparable to each other and the normal modes become strongly non-orthogonal over a broad range of angles. This frequency, called the second vacuum frequency (the first vacuum frequency is near the cyclotron frequency), depends on the magnetic field B and plasma number density N: $\omega_{c2} \sim N^{1/2} B^{-1}$ for $B \ll B_c$ and $\omega_{c2} \sim N^{1/2} B^{-1/2}$ for $B \gg B_c$. Vacuum polarization does not change the polarization-averaged cross-section, but it does change the normal modes and redistribute the total cross-section between them: when $\omega \approx \omega_{c2}$, $\sigma_1 \approx \sigma_2 \approx \sigma_T$. At any particular density the cross-section is unusually high for a narrow range of frequencies (see Fig. 1, later). Conversely, if we assume that most of the flux is transported in the lower cross-section mode, for any photon frequency there is a density at which the cross-section is high. Thus the optical depth seen by a photon is greater than it would be in the absence of the enhanced cross-section at ω_{c2}. Because the resonance frequency varies with density, in an atmosphere of varying density the vacuum resonance has an effect on the spectrum in a wide range of photon energies.

Here we expand on results first presented by Miller & Bulik (1996). In Section 2 we give the normal modes and cross-sections for photons in a strongly magnetized plasma, including the effects of a significant electron–positron pair density and of magnetic fields $B > B_c$. In Section 3 we give a qualitative derivation of the upper and lower bounds to the vacuum resonance feature as a function of magnetic field, scaleheight, and the fraction of positrons. In Section 4 we describe our numerical method for following photons as they scatter through the atmosphere. We also give the results of these simulations, and show that an absorption-like feature is present at reasonable optical depths for any magnetic field $B \gtrsim B_c$. We neglect the effects of photon splitting; at the energies $\hbar\omega \lesssim 50$ keV of interest here, the probability of photon splitting within $\sim 10^6$ cm is small (see Adler 1971). We likewise ignore proton cyclotron scattering, because we focus on scaleheights $l \lesssim 1000$ cm at a constant magnetic latitude, implying that proton cyclotron scattering will yield extremely narrow features, $\Delta\omega/\omega \ll 1$ per cent, which would be unresolvable by current detectors. Finally, in Section 5 we discuss how our results, combined with observations, can constrain physical parameters in SGRs.

2 VACUUM POLARIZATION EFFECTS

It is convenient to describe radiative transfer in a magnetized medium in terms of normal modes. Including both the electric permittivity tensor ϵ and the magnetic permeability tensor μ, the dispersion equation becomes

$$\boldsymbol{k} \times [\mu^{-1}(\boldsymbol{k} \times \boldsymbol{E})] + \frac{\omega}{c} \epsilon \boldsymbol{E} = 0, \tag{1}$$

where $\boldsymbol{E}$ is the electric field. A simple and elegant way of solving equation (1), describing the normal modes and calculating cross-sections, has been introduced by Gnedin & Pavlov (1974). Given a system of coordinates with the magnetic field along the z-axis, and the wave vector in the yz-plane at an angle θ to the magnetic field, we define

$$n_I \equiv 1 + \tfrac{1}{4}(\epsilon_{xx} + \epsilon_{yy} \cos^2\theta + \epsilon_{zz} \sin^2\theta - \epsilon_{xz} \sin 2\theta - \mu_{xx}^{-1} - \mu_{yy}^{-1} \cos^2\theta - \mu_{zz}^{-1} \sin^2\theta + \mu_{xz}^{-1} \sin 2\theta), \tag{2}$$

$$n_L \equiv \tfrac{1}{4}(\epsilon_{xx} - \epsilon_{yy} \cos^2\theta - \epsilon_{zz} \sin^2\theta + \epsilon_{xz} \sin 2\theta + \mu_{xx}^{-1} - \mu_{yy}^{-1} \cos^2\theta - \mu_{zz}^{-1} \sin^2\theta + \mu_{xz}^{-1} \sin 2\theta), \tag{3}$$

and

$$n_C \equiv \frac{\mathrm{i}}{2}(\epsilon_{xy} \cos\theta + \epsilon_{xz} \sin\theta), \tag{4}$$

where μ_{ab}^{-1} is the ab-component of the inverse μ-tensor. The roots of the dispersion equation are

$$n_j = n_I \pm \sqrt{n_L^2 + n_C^2}, \tag{5}$$

where $j = 1, 2$ indicates which normal mode is selected. The refraction coefficients are given by the real part of n_j, and the total absorption coefficients are proportional to the imaginary part of n_j; $\xi_j = (2\omega/c)\,\mathrm{Im}(n_j)$, and the cross-sections in the two modes are

$$\sigma_j = (2\omega/cN_e)\,\mathrm{Im}(n_j). \tag{6}$$

The polarization of the normal modes can be described by the position angle χ_j between the major axis of the polarization ellipse and the projection of the magnetic field $\boldsymbol{B}$ on the plane perpendicular to the wave vector $\boldsymbol{k}$, and the ellipticity $\mathscr{P}$, the modulus of which is equal to the ratio of the minor axis to the major axis of the polarization ellipse, and the sign of which determines the direction of rotation of the electric field. The ellipticity and position angle are

$$\mathscr{P}_j = \frac{r_j - 1}{r_j + 1}, \qquad r_j \exp(2\mathrm{i}\chi_j) = \frac{-n_C \pm \sqrt{n_L^2 + n_C^2}}{n_L}, \tag{7}$$

The polarization vectors can be described by a complex variable b, or by two real parameters q and p:

$$b \equiv q + \mathrm{i}p = \frac{n_L}{n_C}. \tag{8}$$

A detailed discussion of the polarization of the normal modes is given by Pavlov, Shibanov & Yakovlev (1980).

Using the cyclic coordinates $e_{\pm}=2^{-1/2}(e_x \pm \mathrm{i}e_y)$, $e_0=e_z$ (Mészáros 1992, p. 95), the polarization vectors are

$$e^j_{\pm}=\frac{1}{\sqrt{2}}C_j \mathrm{e}^{\mp \mathrm{i}\phi}(K_j \cos\theta \pm 1),$$

$$e^j_0=C_jK_j \sin\theta, \tag{9}$$

where

$$K_j=b[1+(-1)^j(1+b^{-2})^{1/2}] \tag{10}$$

and $C_j=(1+|K_j|^2)^{-1/2}$ is the normalization. It should be noted that in general K_j is complex.

2.1 Vacuum effects in the absence of matter

In the presence of a strong magnetic field the vacuum acquires a non-zero polarizability tensor owing to the existence of virtual electron–positron pairs, so that the permittivity tensor ϵ_{ij} and the magnetic permeability tensor μ_{ij} of the vacuum become different from unity. Charge symmetry implies that both ϵ_{ij} and μ_{ij} are diagonal in a vacuum.

For example, if $B \ll B_c$ and $\hbar\omega \ll mc^2$, so that photon splitting and the creation of real pairs can be neglected, the dielectric tensor and magnetic permeability tensor are given by

$$\epsilon_{ab}-1=\begin{pmatrix} -2a & 0 & 0 \\ 0 & -2a & 0 \\ 0 & 0 & 5a \end{pmatrix}, \tag{11}$$

$$\mu^{-1}_{ab}-1=\begin{pmatrix} -2a & 0 & 0 \\ 0 & -2a & 0 \\ 0 & 0 & -6a \end{pmatrix}, \tag{12}$$

where

$$a \equiv \frac{\alpha}{45\pi}\left(\frac{B}{B_C}\right)^2$$

and α is the fine-structure constant. Inserting equation (12) into equations (2), (3) and (4) we obtain

$$n^{\mathrm{vac}}_I=1+\frac{11}{4}a \sin^2\theta,$$

$$n^{\mathrm{vac}}_L=-\frac{3}{4}a \sin^2\theta, \tag{13}$$

$$n^{\mathrm{vac}}_C=0.$$

The roots of the dispersion equation in a vacuum are real, and the refraction indices of the normal models are

$$n^{\mathrm{vac}}_1=n^{\mathrm{vac}}_I+n^{\mathrm{vac}}_L=1+2a \sin^2\theta, \tag{14}$$

$$n^{\mathrm{vac}}_2=n^{\mathrm{vac}}_I-n^{\mathrm{vac}}_L=1+\frac{7}{2}a \sin^2\theta. \tag{15}$$

Note that knowledge of the refraction indices n^{vac}_1 and n^{vac}_2 suffices to determine the influence of vacuum polarization on the propagation of light in the presence of matter.

The refraction indices $n^{\mathrm{vac}}_{1,2}$ have been calculated for $\hbar\omega \ll m_ec^2$ and arbitrary magnetic field by Tsai & Erber (1974):

$$n^{\mathrm{vac}}_1=1+\frac{\alpha}{4\pi}\eta_1(h) \sin^2\theta, \tag{16}$$

$$n^{\mathrm{vac}}_2=1+\frac{\alpha}{4\pi}\eta_2(h) \sin^2\theta, \tag{17}$$

where

$$h \equiv \frac{B}{B_c},$$

and

$$\eta_1(h)=8 \ln\Gamma_1(1+h)-4h \ln\Gamma(1+h)-\frac{2}{3}\Psi(1+h) - 2h \ln h-2h^2+2h \ln(2\pi)+\frac{1}{3h}+\frac{1}{3}-8L_1, \tag{18}$$

$$\eta_2(h)=-4h \ln\Gamma(1+h)+4h^2\Psi(1+h)+2h \ln h + 2h[\ln(2\pi)-1]-4h^2+\frac{2}{3}. \tag{19}$$

In these expressions, $\Psi(x)=\mathrm{d}/\mathrm{d}x \ln\Gamma(x)$,

$$\ln\Gamma_1(x)=\int_0^x \mathrm{d}t \ln\Gamma(t)+\frac{x}{2}[x-1-\ln(2\pi)], \tag{20}$$

and $L_1=\frac{1}{3}+\int_0^1 \mathrm{d}x \ln\Gamma_1(1+x)\approx 0.249$. The asymptotic limits of the functions $\eta_{1,2}(h)$ have been found by Tsai & Erber (1975). In the low-field limit, $B \ll B_c$,

$$\eta_1(h)\approx\frac{14}{45}h^2-\frac{13}{315}h^4, \tag{21}$$

$$\eta_2(h)\approx\frac{8}{45}h^2-\frac{379}{5040}h^4, \tag{22}$$

and, when $B \gg B_c$,

$$\eta_1(h)\approx\frac{2}{3}h+\left(\frac{1}{3}+\frac{2}{3}\gamma-8L_1\right), \tag{23}$$

$$\eta_2(h)\approx\frac{2}{3}-h^{-1} \ln(2h), \tag{24}$$

where $\gamma=0.577\ldots$ is Euler's constant.

Using equations (14) and (15) we can rewrite equations (13):

$$n^{\mathrm{vac}}_I=\frac{1}{2}(n^{\mathrm{vac}}_1+n^{\mathrm{vac}}_2) =1+\frac{\alpha}{8\pi}\sin^2\theta[\eta_1(h)+\eta_2(h)], \tag{25}$$

$$n_L^{\rm vac}=\frac{1}{2}\,(n_1^{\rm vac}-n_2^{\rm vac})=\frac{\alpha}{8\pi}\sin^2\theta[\eta_1(h)-\eta_2(h)], \tag{26}$$

$$n_C^{\rm vac}=0. \tag{27}$$

The normal modes are polarized linearly for all angles of propagation except for the degenerate case of propagation along the direction of the field when they are circular. Such a behaviour could also be found by considering the symmetry of the problem.

2.2 Propagation of radiation in a system with matter present

Consider now a system in which the plasma density is low enough that the contribution of plasma to the dielectric tensor is $|e_{ij}^{\rm p}-1|\ll 1$, and the magnetic field is small so that $|\epsilon_{ij}^{\rm vac}-1|\ll 1$ and $|\mu_{ij}^{-1}-1|\ll 1$. This condition is satisfied for $B/B_{\rm c}<40$ and $\omega_{\rm p}^2\ll\omega_B\omega$, which hold for

$$\frac{\hbar\omega}{mc^2}\gg 1.6\times 10^{-8}\left(\frac{N_{\rm e}}{10^{24}\ {\rm cm}^{-3}}\right)\left(\frac{B_{\rm c}}{B}\right). \tag{28}$$

Such a system can be described by the dielectric tensor

$$\epsilon_{ab}=\epsilon_{ab}^{\rm vac}+\epsilon_{ab}^{\rm p}-\delta_{ab}, \tag{29}$$

and the vacuum permeability tensor. The plasma dielectric tensor can be expressed as

$$\epsilon_{ab}=\delta_{ab}-\left(\frac{\omega_{\rm p}^2}{\omega^2}\right)\Pi_{ab},$$

where

$$\omega_{\rm p}=\left(\frac{4\pi Ne^2}{m}\right)^{1/2}$$

is the plasma frequency and Π_{ab} is the plasma polarization tensor. The plasma polarization tensor is diagonal in the cyclic coordinates, and for cold electron plasma is given by

$$\Pi_{\alpha\alpha}=\frac{\omega}{\omega+\alpha\omega_B-{\rm i}\gamma_{\rm r}}=\frac{\omega}{\omega_{\rm t}+\alpha\omega_B}, \tag{30}$$

where $\alpha=-1,0,+1$, and $\gamma_{\rm r}=(2/3)(e^2/mc^3)\,\omega^2$ is the radiative width, and we denote $\omega_{\rm t}=\omega-{\rm i}\gamma_{\rm r}$. When there is an admixture of pairs, such that the positron fraction is $f\equiv n_{e^+}/(n_{e^-}+n_{e^+})$, the cyclic components of the polarization tensor are modified:

$$\Pi_{\alpha\alpha}^f=f\,\Pi_{\alpha\alpha}+(1-f)\,\Pi_{-\alpha-\alpha}. \tag{31}$$

Inserting equation (30) into equations (3) and (4), we obtain

$$n_I=1+\frac{1}{4}\,\frac{\omega_{\rm p}^2}{\omega}\left[(1+\cos^2\theta)\,\frac{\omega_{\rm t}}{\omega_{\rm t}^2-\omega_B^2}+\sin^2\theta\,\frac{1}{\omega_{\rm t}}\right]$$

$$+\frac{\alpha}{8\pi}\sin^2\theta[\eta_1(h)+\eta_2(h)], \tag{32}$$

$$n_L=-\frac{\sin^2\theta}{4}\left\{\frac{\omega_{\rm p}^2}{\omega\omega_{\rm t}}\,\frac{\omega_B^2}{\omega_{\rm t}^2-\omega_B^2}+\frac{\alpha}{2\pi}\,[\eta_1(h)-\eta_2(h)]\right\} \tag{33}$$

and

$$n_C=-\frac{1}{2}\,\frac{\omega_{\rm p}^2}{\omega}\left(\frac{\omega_B}{\omega_{\rm t}^2-\omega_B^2}\right)\cos\theta. \tag{34}$$

When $f\neq 0$, the parameter n_L is not changed, whereas

$$n_C=-\left(\frac{1-2f}{2}\right)\frac{\omega_{\rm p}^2}{\omega^2}\,\frac{\omega\omega_B}{\omega_{\rm t}^2-\omega_B^2}\cos\theta. \tag{35}$$

Inserting equations (33) and (34) into equation (8), and neglecting terms proportional to $\gamma_{\rm r}^2$, we obtain

$$q=\frac{1}{1-2f}\,\frac{\sin^2\theta}{2\cos\theta}\,\frac{\omega_B}{\omega}$$

$$\times\left\{1+\frac{\alpha}{2\pi}\,[\eta_1(h)-\eta_2(h)]\,\frac{\omega^2}{\omega_{\rm p}^2}\left(\frac{\omega^2}{\omega_B^2}-1\right)\right\} \tag{36}$$

and

$$p=\frac{1}{1-2f}\,\frac{\sin^2\theta}{2\cos\theta}\,\frac{\omega_B\gamma_{\rm r}}{\omega^2}\left\{1-\frac{\alpha}{\pi}\,[\eta_1(h)-\eta_2(h)]\,\frac{\omega^2}{\omega_{\rm p}^2}\right\}. \tag{37}$$

The normal modes are linear and orthogonal for most frequencies and angles, since $q^2\gg p^2$ for most of the parameter space. The absorption coefficients in this regime can be obtained by inserting equations (32), (33) and (34) into (5), and noting that the ratio n_L/n_C is large and real. Thus we obtain

$$\xi_1=N\sigma_{\rm T}\sin^2\theta, \tag{38}$$

$$\xi_2=N\sigma_{\rm T}\left(\frac{\omega}{\omega_B}\right)^2. \tag{39}$$

The critical points are where $q(\omega)=0$. Such points exist when

$$\frac{\alpha}{8\pi}\,\frac{\omega_B^2}{\omega_{\rm p}^2}\,[\eta_1(h)-\eta_2(h)]>1. \tag{40}$$

Generally, for a system consisting of electron plasma and magnetized vacuum, there exist two frequencies for which $q(\omega)=0$, one very close to the cyclotron frequency, and the other at $\omega\ll\omega_B$. In this work we will be interested in the latter. At this point, called the second vacuum frequency, the normal modes are circular for most propagation angles. This leads to an increase of the absorption of the low-cross-section mode and a simultaneous decrease of the absorption in the high-cross-section mode. From equation (36), the second vacuum frequency is

$$\omega_{c2}=\omega_{\rm p}\left\{\frac{\alpha}{2\pi}\,[\eta_1(h)-\eta_2(h)]\right\}^{-1/2}, \tag{41}$$

with the limits

$$\hbar\omega_{c2}=\hbar\omega_{\rm p}(15\pi/\alpha)^{1/2}(B_{\rm c}/B)$$

$$=30N_{26}^{1/2}(B_{\rm c}/B)\ {\rm keV} \tag{42}$$

for $B \ll B_c$, and

$$\hbar\omega_{c2} = \hbar\omega_p (3\pi/\alpha)^{1/2} (B_c/B)^{1/2} = 13 N_{26}^{1/2} (B_c/B)^{1/2} \text{ keV} \quad (43)$$

for $B \gg B_c$, where $N_{26} \equiv N/10^{26}$ cm^{-3}. Polarization of the normal modes at ω_{c2} is determined by the parameter p. The modes are circular when $p^2 < 1$ and linear when $p^2 > 1$. In the case when $p = 1$ and $q = 0$, the two polarization modes coincide. Inserting equation (41) into (37), we obtain the value of p at the vacuum frequency

$$p(\omega_{c2}, \theta) = \frac{\alpha}{1-2f} \frac{\sin^2\theta}{3\cos\theta} \frac{\hbar\omega_B}{mc^2}. \quad (44)$$

We can define a critical angle θ_c as an angle for which $p(\omega_{c2}, \theta_c) = 1$. For the magnetic fields considered here, θ_c is very close to $\pi/2$; $\pi/2 - \theta_c \approx (\alpha/3)(B/B_c)$ for electron plasma. Again inserting equations (32), (33) and (34) into (5), and noting that the ratio n_L/n_C is imaginary and small for the angles $\theta < \theta_c$, we obtain

$$\xi_{1,2} = N\sigma_T \left[\frac{1}{2}\sin^2\theta + \left(\frac{\omega}{\omega_c}\right)^2 \frac{1+\cos^2\theta}{2} \pm \left(\frac{\omega}{\omega_c}\right)^3 \frac{\cos\theta}{2} \sqrt{1 - \left(\frac{\alpha}{1-2f}\frac{B}{B_c}\right)^2 \frac{\sin^4\theta}{9\cos^2\theta}} \right]. \quad (45)$$

In the case of propagation orthogonal to the field, when $\theta > \theta_c$, the normal modes become linear and the absorption coefficients are given by equations (38) and (39).

The width of the resonance is associated with the extent of the interval where $q(\omega, \theta) < 1$. It can be estimated as the inverse of the derivative of q at the vacuum frequency:

$$\nu_{vac} = \left(\left.\frac{dq}{d\omega}\right|_{\omega_{c2}} \right)^{-1} = (1-2f) \frac{\cos\theta}{\sin^2\theta} \frac{\omega_{c2}^2}{\omega_B}. \quad (46)$$

The vacuum frequency and the shape of the vacuum resonance do not depend on temperature, since thermal effects alter the dielectric tensor weakly for $\omega \ll \omega_B$. Unlike the cyclotron resonance, the vacuum resonance is a result of *global* properties of the medium and does not depend on any individual particle resonance.

2.3 Scattering cross-section

Let us now consider scattering in a hot, magnetized plasma. A photon with energy ω, wave vector k propagating at an angle θ to the magnetic field B, and polarization vector e scatters on an electron with parallel momentum p. After the scattering the photon has energy ω', wave vector k' and polarization vector e', and the electron momentum is p'.

The scattering cross-section is given by (Mészáros 1992, p. 131)

$$d\sigma(\omega, \theta, p \mapsto \omega', \theta', p') = r_0^2 \frac{\omega'}{\omega} \frac{m}{|k-k'|} |\langle e|\Pi|e'\rangle|^2, \quad (47)$$

where $r_0 = e^2/mc^2$ is the classical electron radius. After averaging equation (47) over ϕ' we obtain

$$d\sigma(\omega, \theta, p \mapsto \omega', \theta', p') = r_0^2 \frac{\omega'}{\omega} \frac{m}{|k-k'|} \times \sum_\alpha |\Pi_{\pm\alpha}|^2 |e_\alpha|^2 |e'_\alpha|^2, \quad (48)$$

where we have the $+$ sign for scattering on electrons and the $-$ sign for scattering on positrons. The scattering amplitude, with first-order relativistic corrections, are

$$\Pi_+ = 1 - \frac{\omega_B}{\omega' + \omega_B - pk' + k'^2/2 + i\gamma_r},$$

$$\Pi_- = 1 + \frac{\omega_B}{\omega - \omega_B - pk - k^2/2 + i\gamma_r}, \quad (49)$$

$$\Pi_0 = 1 + \frac{(p+k/2)(p-k'+k/2)}{\omega - pk - k^2/2 + i\gamma_r} - \frac{(p-k'/2)(p-k'+k/2)}{\omega' - pk' + k'^2/2 + i\gamma_r}.$$

Assuming coherent scattering, i.e. $k = k'$, we average over the final states and use the polarization normal modes to obtain the total cross-section from one mode to another:

$$\sigma_{ij} = \sigma_T \sum_\alpha |e^i_\alpha|^2 |\Pi_{\pm\alpha}|^2 A^j_\alpha, \quad (50)$$

where

$$A^j_\alpha = \frac{3}{4} \int d\cos\theta |e^j_\alpha|^2.$$

In general the integrals A^j_α are difficult to calculate analytically. We can introduce the mode switching probability for the two modes:

$$p_{ij} = \frac{\sigma_{ij}}{\sigma_{ij} + \sigma_{jj}}. \quad (51)$$

We will find the cross-section and the mode switching probabilities in some limiting cases.

When polarization modes are linear for most of the angles, e.g. outside the resonance, where polarization is vacuum-dominated, we have $|b| = |n_L/n_c| \gg 1$, and we find using equation (10) that $K_1 \to 2b$, $K_2 \to -1/2b$, $C_1 \to 1/2b$, and $C_2 \to 1$. The components of the two polarization modes are then

$$e^1_\pm \approx \frac{1}{\sqrt{2}} \cos\theta e^{\mp i\phi}, \qquad e^1_z \approx \sin\theta, \quad (52)$$

and

$$e^2_\pm \approx \pm\frac{1}{\sqrt{2}} e^{\mp i\phi}, \qquad e^2_z \approx 0. \quad (53)$$

The total scattering cross-sections in the limit $u \equiv (\omega_B/\omega)^2 \gg 1$ of photons at initial incident angle θ to the magnetic field are

$$\sigma_{1\to1}\approx\sigma_{\rm T}\sin^2\theta, \tag{54}$$

$$\sigma_{1\to2}\approx\frac{3}{4}\sigma_{\rm T}\frac{1}{u}\cos^2\theta, \tag{55}$$

$$\sigma_{2\to1}\approx\frac{1}{4}\sigma_{\rm T}\frac{1}{u}, \tag{56}$$

$$\sigma_{2\to2}\approx\frac{3}{4}\sigma_{\rm T}\frac{1}{u}. \tag{57}$$

Thus the probability of switching from the high-cross-section mode to the low-cross-section mode is

$$p_{1\to2}=\frac{\frac{3}{4}\cos^2\theta}{u\sin^2\theta+\frac{3}{4}\cos^2\theta}\approx\frac{3}{4}\left(\frac{\omega}{\omega_B}\right)^2\cot^2\theta, \tag{58}$$

where the last approximation holds when $\theta\gg\sqrt{3/2}\,(\omega/\omega_B)$. The probability of switching from the low-cross-section mode to the high-cross-section mode is

$$p_{2\to1}=\frac{1}{4}. \tag{59}$$

In contrast, when $b\ll1$, which holds for most of the propagation angles in the resonance ($\theta<\theta_{\rm c}$), the modes are circular, and $K_1\to1$, $K_2\to-1$, $C_1\to1/\sqrt{2}$, and $C_2\to1/\sqrt{2}$. The components of the two modes are then

$$e^1_\pm\approx\pm\frac{1}{2}\,{\rm e}^{\mp{\rm i}\phi}(1\mp\cos\theta),\qquad e^1_z\approx-\frac{1}{\sqrt{2}}\sin\theta, \tag{60}$$

and

$$e^2_\pm\approx\pm\frac{1}{2}\,{\rm e}^{\mp{\rm i}\phi}(1\pm\cos\theta),\qquad e^2_z\approx-\frac{1}{\sqrt{2}}\sin\theta. \tag{61}$$

The total scattering cross-section in the limit $u\gg1$ for any initial or final polarization state is then, in the limit $\sin\theta\gg u^{-1/2}$,

$$\sigma_{{\rm i}\to{\rm f}}\approx\frac{1}{4}\sigma_{\rm T}\sin^2\theta. \tag{62}$$

The mode switching probabilities are

$$p_{1\to2}=p_{2\to1}=\frac{1}{2}. \tag{63}$$

We calculate the polarization of the normal modes using the cold plasma approximation, since the thermal effects are not important in the range of energies far from the cyclotron resonance. We then use equation (48) and the scattering amplitudes (49) to find the cross-section as a function of the final angle. We present the scattering cross-section as a function of photon energy in the left-hand panel of Fig. 1. In the right-hand panel of Fig. 1 we show the mode switching probabilities for the two modes. The insets show details in the vicinity of the vacuum resonance. Note that the low- to high-cross-section mode switching probability is enhanced around the vacuum resonance and reaches nearly unity. Because of this, scattering in the low mode can be dominated by mode switching, as it is in many of the results that we describe in Section 4.

Absorption can also contribute significantly to the opacity over the frequencies and densities of interest, depending on the composition of the surface layers and magnetosphere. If the primary atom has a high atomic number, e.g. silicon or iron, then even when $kT=20$ keV the atoms will not be completely ionized (atomic binding energies are increased greatly by strong magnetic fields). If the primary atom is hydrogen or helium, virtually all atoms will be completely ionized and only scattering and free–free absorption contribute to the opacity. Here we assume that only lighter elements are present, so that bound–free and bound–bound absorption may be ignored.

Given this assumption, scattering dominates the opacity over most of the photosphere. Free–free absorption can, however, be important for the lower photon energies. The free–free absorption cross-section in the low-cross-section mode is (see e.g. Mészáros 1992)

$$\sigma_{\rm abs}\approx4\times10^{-28}\left(\frac{B_{\rm c}}{B}\right)^{-2}N_{26}T_8^{-1/2}\omega_{10}^{-1}\ {\rm cm}^2, \tag{64}$$

where $T_8\equiv T/10^8$ K and $\omega_{10}\equiv\hbar\omega/10$ keV. When the photon energy $\hbar\omega<kT$, induced scattering and absorption are important, and we include this by multiplying the total interaction cross-section by the factor

$${\rm e}^{\hbar\omega/kT}/({\rm e}^{\hbar\omega/kT}-1).$$

2.4 Summary of the effects of vacuum polarization

We have shown above that vacuum polarization affects strongly the scattering cross-section for the two modes. However, vacuum polarization does not introduce additional absorption. As can be seen from equations (6) and (5), the polarization-averaged cross-section depends only on the imaginary part of n_I. From equation (32), the vacuum contribution, represented by the third term in this equation, is real. Moreover, the imaginary part of n_I is proportional to $N_{\rm e}$. Therefore, from equation (6), the polarization-averaged cross-section depends neither on plasma density nor on vacuum polarization. The main effect of vacuum polarization is redistribution of the cross-section between the two modes. The effects described here will not be seen in calculations that use polarization-averaged cross-sections.

For example, the scattering cross-section in the O-mode has no resonance at the cyclotron frequency when the vacuum effects are negligible (Ventura et al. 1979). Since radiative transfer takes place predominantly in the low-cross-section mode, neglecting vacuum polarization would inhibit formation of cyclotron lines in the polarization-averaged spectra.

Vacuum polarization alters the mode switching probabilities, which also influences radiative transfer. In the case considered here, the increase of $p_{2\to1}$ to almost unity in the wings of the resonance also increases the number of scatterings that a photon undergoes before leaving. This increases the chances of absorption, and enhances the effects of Comptonization.

3 QUALITATIVE TREATMENT OF SCATTERING WITH THE SECOND VACUUM FREQUENCY

From Section 2 it is clear that the scattering cross-section depends strongly on the parameter

$$b \approx \frac{\sin^2\theta}{2\cos\theta}\frac{\omega_B}{\omega}\frac{1}{(1-2f)} \times\left\{1-\frac{\alpha}{2\pi}\left(\frac{\omega}{\omega_p}\right)^2[\eta_1(h)-\eta_2(h)]\right\}. \quad (65)$$

When $|b|\ll 1$ the cross-section is $\sim\sigma_T$ in either polarization mode, whereas when $|b|\gg 1$ one mode has $\sigma\ll\sigma_T$. Because $\omega_{c2}\sim N^{1/2}$, as radiation propagates from regions of high density to regions of low density the resonance frequency changes. In effect, the resonance acts as a sliding window of high opacity. Qualitatively, we expect that the resonance will have an impact on the flux at a given frequency if (i) the optical depth through the resonance is greater than unity, and (ii) the optical depth to the surface without the resonance is less than unity. These requirements give us, respectively, the minimum and maximum photon energies at which the vacuum resonance changes the spectrum.

We can estimate the fractional width ϵ of the resonance by arbitrarily setting the bound between $|b|\ll 1$ and $|b|\gg 1$ at $|b|=1$ and demanding that, at $\omega=\omega_{c2}(1\pm\epsilon)$, $|b|=1$. This gives

$$\epsilon=\frac{\omega_{c2}}{\omega_B}(1-2f)\frac{\cos\theta}{\sin^2\theta}=0.02h^{-1}\omega_{10}\frac{\cos\theta}{\sin^2\theta}(1-2f), \quad (66)$$

which is identical to equation (46). If $\epsilon\ll 1$ and the atmosphere is exponential with scaleheight ℓ, then the thickness of the resonance is $\approx 4\epsilon\ell$. Assuming that the resonance cross-section is $\sigma\approx\sigma_T\sin^2\theta$, if the magnetic field is parallel

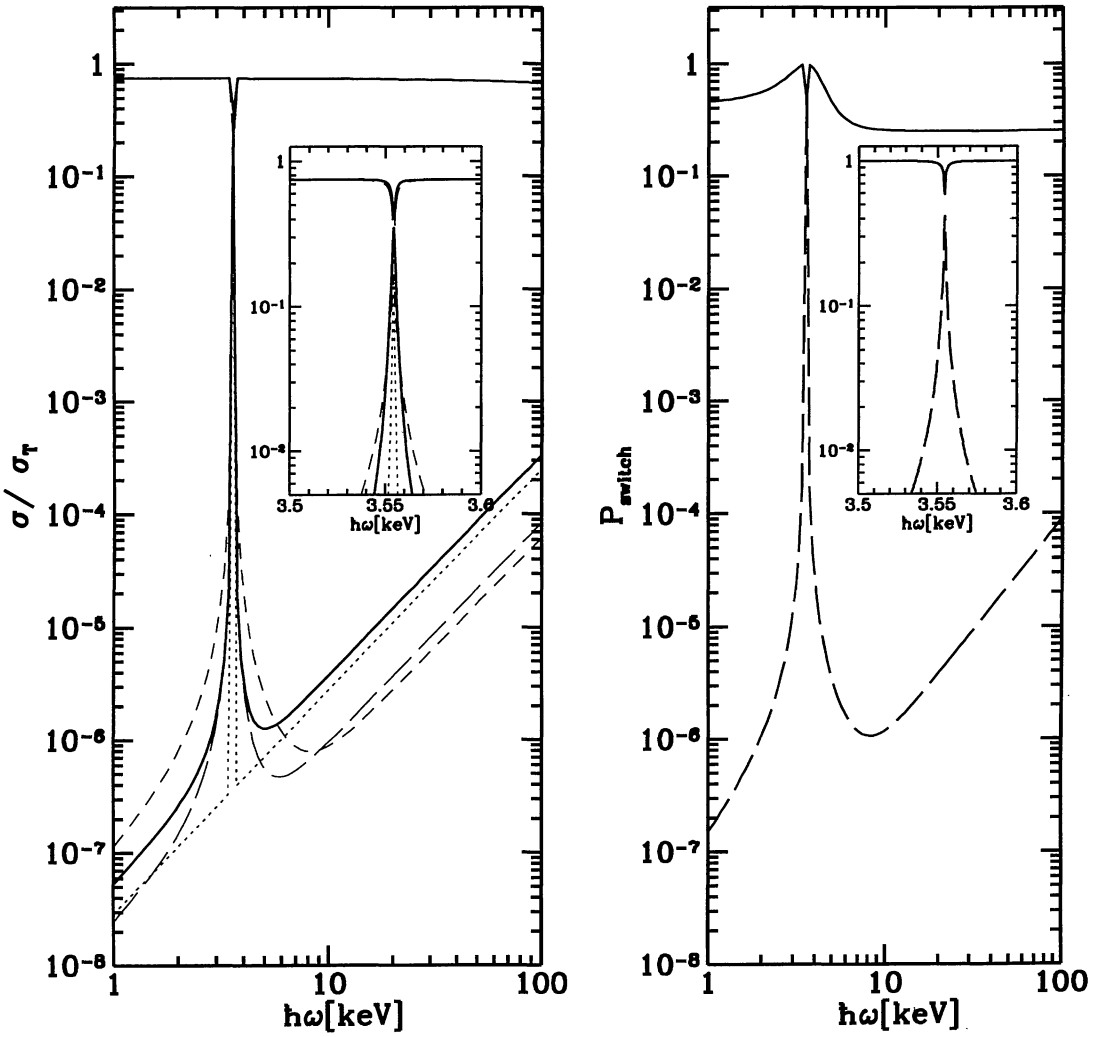

Figure 1. Left-hand panel: scattering cross-section, in units of the Thomson cross-section, versus photon energy. The solid lines correspond to the total cross-sections in the two modes. The dotted line represents the cross-section for the low mode to the low mode, the long-dashed line represents the low- to high-mode cross-section, and the short-dashed line represents the high-mode to low-mode cross-section; the high to high cross-section is essentially equal to the total high mode cross-section. Note that the width of the resonance in the low- to high-mode cross-section exceeds that in the low to low cross-section. The inset shows a close-up of the frequency range near the resonance. Right-hand panel: mode switching probabilities for the low mode (solid line), and the high mode (dashed line).

to the surface normal then the optical depth through the resonance is $\tau = N(4\epsilon\ell)\sigma_T \sin^2\theta/\cos\theta$:

$$\tau = 6h\ell_1\omega_{10}^3(1-2f), \qquad B \ll B_c, \tag{67}$$

$$\tau = 30\ell_1\omega_{10}^3(1-2f), \qquad B \gg B_c, \tag{68}$$

where $\ell_1 \equiv (l/10\ \mathrm{cm})$. This gives the lower bound to the feature. To estimate the photon energy at which the optical depth without the resonance is unity, we solve

$$n\sigma_T\left(\frac{\sin^2\theta}{\cos\theta}\right)\left(\frac{\omega}{\omega_B}\right)^2 \ell = 1, \tag{69}$$

which gives $\hbar\omega \approx 30\ell_1^{-1/4}$ keV when $B \ll B_c$ and $\hbar\omega \approx 20\ell_1^{-1/4}h^{1/4}$ keV when $B \gg B_c$.

To summarize, when the magnetic field is parallel to the surface normal then when $B \gg B_c$ this simple analytical treatment gives lower and upper bounds ω_l and ω_h of

$$\hbar\omega_l \approx 6h^{-1/3}\ell_1^{-1/3}(1-2f)^{-1/3}\ \mathrm{keV}, \tag{70}$$

$$\hbar\omega_h \approx 30\ell_1^{-1/4}(\sin\theta)^{-1}\ \mathrm{keV}, \tag{71}$$

whereas, for $B \gg B_c$,

$$\hbar\omega_l \approx 3\ell_1^{-1/3}(1-2f)^{-1/3}\ \mathrm{keV}, \tag{72}$$

$$\hbar\omega_h \approx 20\ell_1^{-1/4}h^{1/4}(\sin\theta)^{-1}\ \mathrm{keV}. \tag{73}$$

The scalings with magnetic field, scaleheight and f are confirmed by our numerical results: typically $\hbar\omega_l \approx 5$ keV and $\hbar\omega_h \approx 40$ keV, if the radiation is produced very deep in the atmosphere.

4 NUMERICAL METHOD AND RESULTS

4.1 Method

Following the procedure outlined in Section 2.3 to generate cross-sections, and adding the corrections mentioned there for free–free absorption and induced Compton scattering, we use an adaptive mesh to produce a table of physical depth as a function of optical depth for various values of the magnetic field and scaleheight. The physical depth depends on both the frequency and the direction of the photon, and

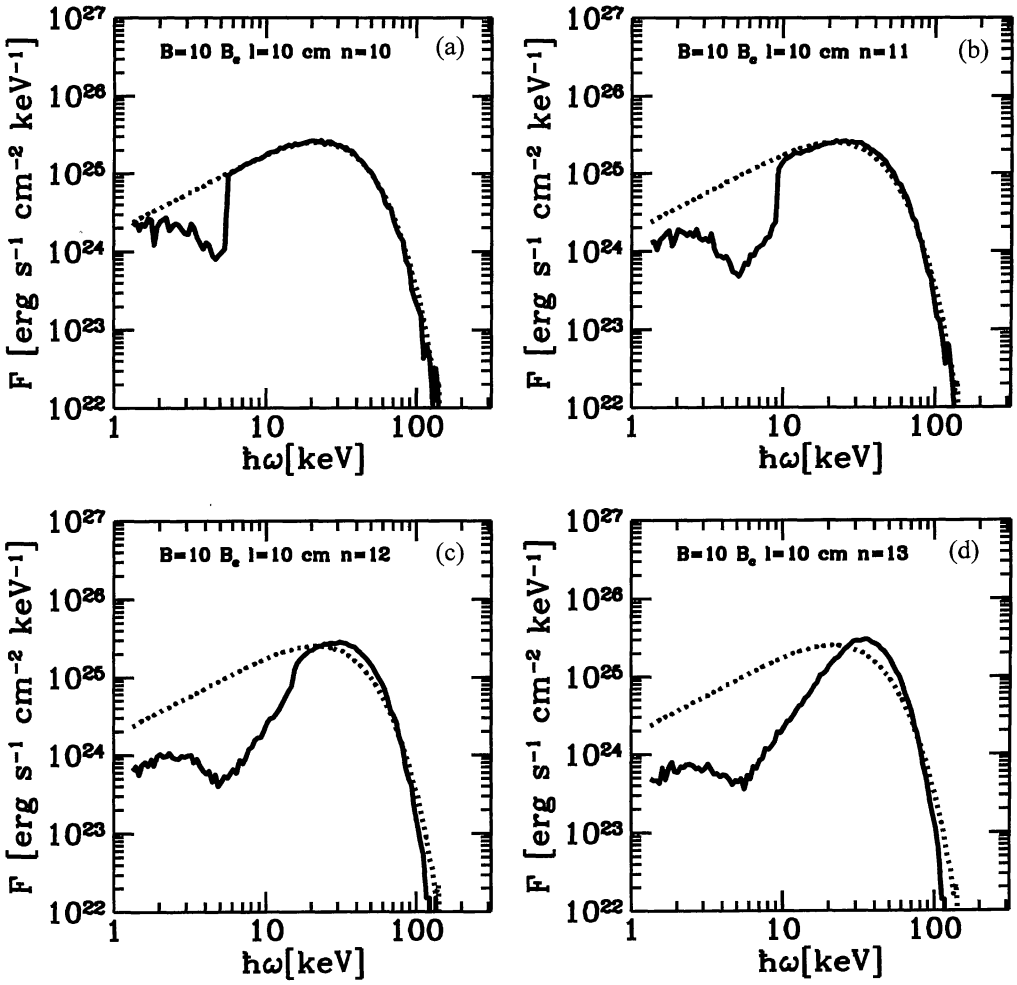

Figure 2. Model spectra, as seen at the stellar surface (solid lines), showing the effects of varying photon production depth. The input spectrum in each case is a 10-keV blackbody (dotted lines), and the magnetic field is perpendicular to the surface. The magnetic field for all four panels is $B = 10B_c$, the scaleheight is $l = 10$ cm, and the pair fraction is $f = 0$. In panels (a), (b), (c) and (d), respectively, the photons are produced at 10, 11, 12 and 13 scaleheights, where the number density at the surface is 6×10^{21} cm^{-3} (corresponding to 10^{-2} g cm^{-3} for a fully ionized hydrogen plasma). Note that the low-energy bound of the feature remains roughly constant, whereas the high-energy bound increases with increasing production depth.

in particular for angles nearly perpendicular to the direction of the magnetic field the vacuum resonance feature is very sharp, and thus must be integrated carefully. We achieve sufficient accuracy with 130 logarithmically spaced zones in photon frequency from $\hbar\omega = 10^{-2.6} m_e c^2$ to $\hbar\omega = m_e c^2$, 50 linearly spaced zones in angle, and optical depths from 10^{-1} to 10^4, logarithmically spaced.

To produce a spectrum, we use a Monte Carlo code to pass 100 000 photons through the atmosphere, starting each photon at a single layer deep in the atmosphere. For each scattering we generate an optical depth travelled, which combined with the direction and with the table of physical depth versus optical depth gives the new physical depth of the photon. If the photon escapes from the atmosphere we store its energy and propagation direction. Otherwise, we use the differential cross-section to select its new energy and angle and determine whether the photon switches polarization modes, and repeat the process.

It is essential to include the effects of Comptonization and the mode switching in these simulations. At temperatures of ~ 10 keV the energy change of a photon in a single scattering is much greater than the width of the vacuum resonance. Thus, in the >50 per cent of scatterings in the resonance when the photon switches modes, the photon will be Comptonized out of the resonance and may require several thousand scatterings to return to the low-cross-section mode, during which its fractional energy change can be of order unity and in the course of which the photon is likely to be absorbed. We account for the effects of mode switching by checking at each scatter whether the photon switches modes and, if it does, simulating an absorption by drawing the new energy of the photon from a thermal distribution. We do not change the physical depth of the photon in this case, becaue the mean free path in the parallel mode is small enough that the net distance travelled in the parallel mode is negligible. To speed up the program, we also limit the total number of scatterings per photon to 1000; in the results reported here, between 97 and 100 per cent of the photons escape in fewer than 1000 scatterings.

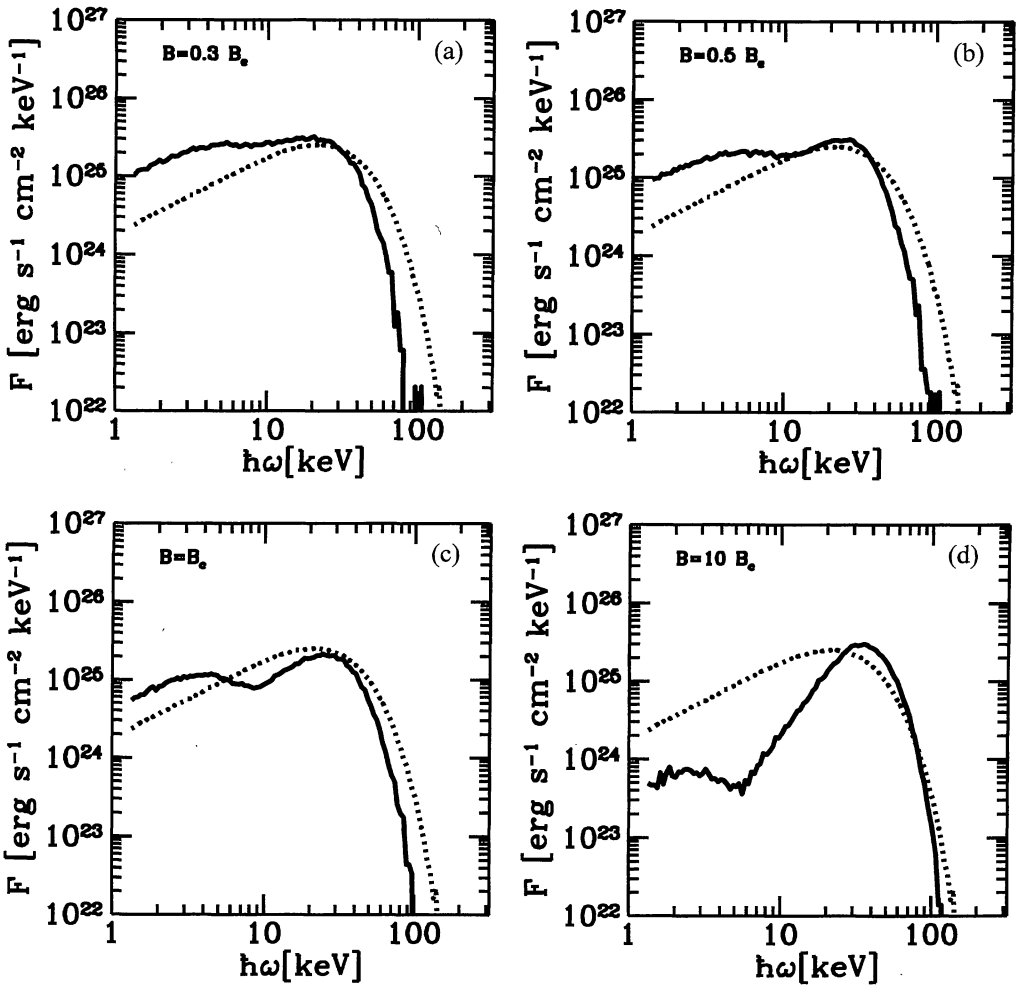

Figure 3. Model spectra, as seen at the stellar surface (solid lines), showing the effects of different magnetic fields. As in Fig. 2, the input (dotted lines) is a 10-keV blackbody, the magnetic field is perpendicular to the surface, $l = 10$ cm, and $f = 0$, and here the photons are assumed to be produced deep in the atmosphere. Panels (a), (b), (c) and (d) respectively, show spectra for magnetic fields of $B = 0.3B_c$, $B = 0.5B_c$, $B = B_c$ and $B = 10B_c$. This figure shows that the absorption-like feature will only be detectable for $B \gtrsim B_c$.

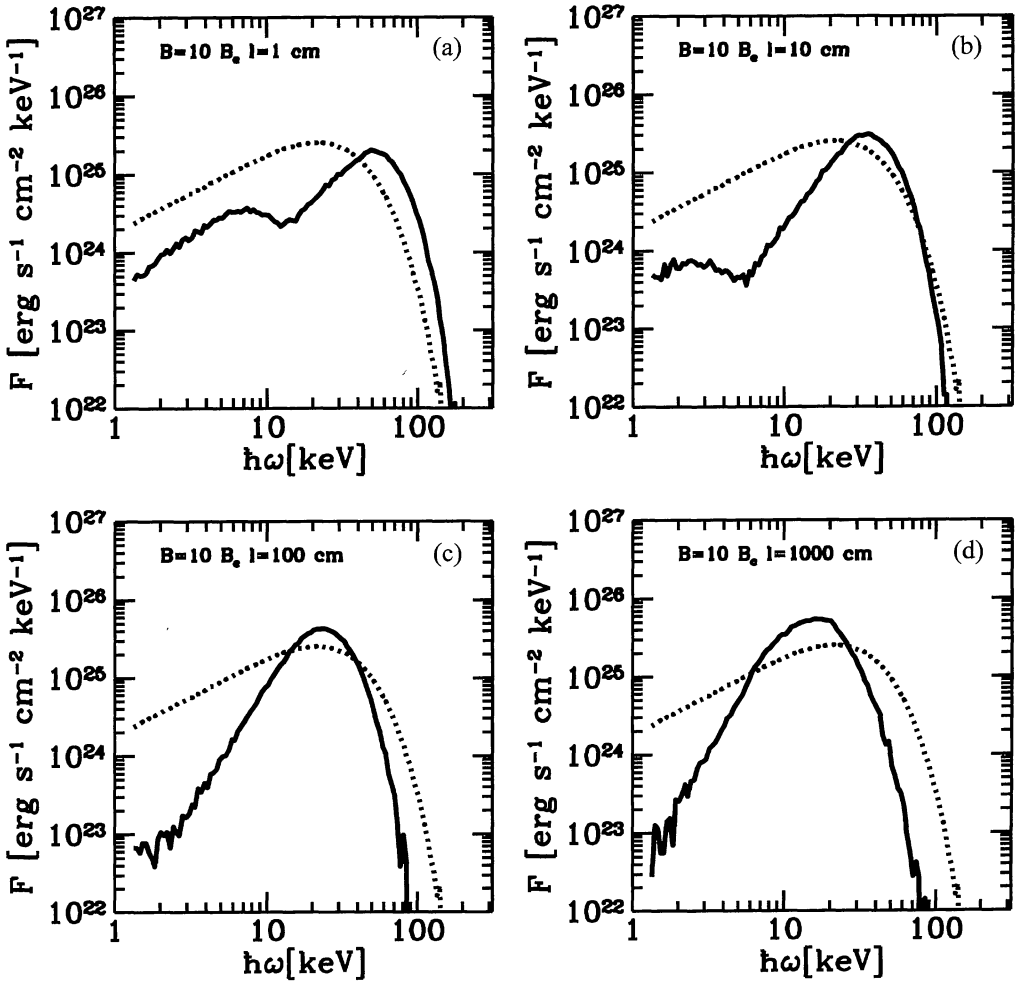

Figure 4. Model spectra, as seen at the stellar surface (solid lines), showing the effects of different scaleheights. Here $B=10B_c$, $f=0$, the input (dotted lines) is a 10-keV blackbody produced deep in the atmosphere, and the magnetic field is perpendicular to the surface. Panels (a), (b), (c) and (d), respectively, show spectra for scaleheights of $l=1$, 10, 100, 1000 cm. Note that the vacuum feature moves to lower energies for large scaleheights. Thus an instrument with a low-energy spectral cut-off of e.g. $\sim$5 keV might see only a low-energy drop-off during a burst when the scaleheight is large, but could see the whole absorption-like feature during the afterglow when the scaleheight has dropped.

4.2 Results

In this section we show spectra for several representative combinations of physical parameters. In every case the input spectrum is a blackbody at 10 keV. Fig. 2 shows a sequence where the production depth of the photons (in units of the scaleheight) changes but the magnetic field is fixed at $B=10B_c$ and the scaleheight is 10 cm. Note that the high-energy fall-off moves to higher energies with greater depth, whereas the low-energy edge of the feature is roughly constant in energy, as predicted by our treatment in Section 3. Fig. 3 shows spectra for different magnetic fields, with $B=0.3$, 0.5, 1.0 and $10B_c$. In these the vacuum resonance feature is only clearly visible for $B\gtrsim B_c$; at lower fields the contrast in cross-section in and out of the vacuum resonance is not enough to create a significant feature. In Fig. 4 we isolate the effects of changing the scaleheight, as ℓ ranges from 1 to 1000 cm. From these we see that the larger the scaleheight, the broader the feature, to the extent that the vacuum resonance may appear as only a fall-off at low and high energies instead of an absorption-like feature. In Fig. 5 we concentrate on the effects of different pair densities. In these graphs $B=10B_c$, the scaleheight is 10 cm, and the production depth is 13 scaleheights. As the fraction f of pairs (defined earlier) increases from 0 to 0.49, the high-energy edge of the feature remains fixed while the low-energy edge moves up, narrowing the trough and making it shallower. Fig. 6 shows our last energy spectrum, in which the magnetic field is in the surface instead of normal to it (as it was in Figs 2–5), and we see that the low-energy part of the spectrum is flatter than it is when the field is along the surface normal.

In Fig. 7 we show the angular distribution of emergent radiation, integrated over all photon energies, for a magnetic field $B=10B_c$ along the surface normal, a scaleheight of 10 cm, and energy generated deep in the atmosphere. For comparison we also show the angular distribution of emergent radiation for isotropic scattering. The radiation is strongly peaked towards the normal; part of this comes from geometric effects (see e.g. Chandrasekhar 1960, section 5),

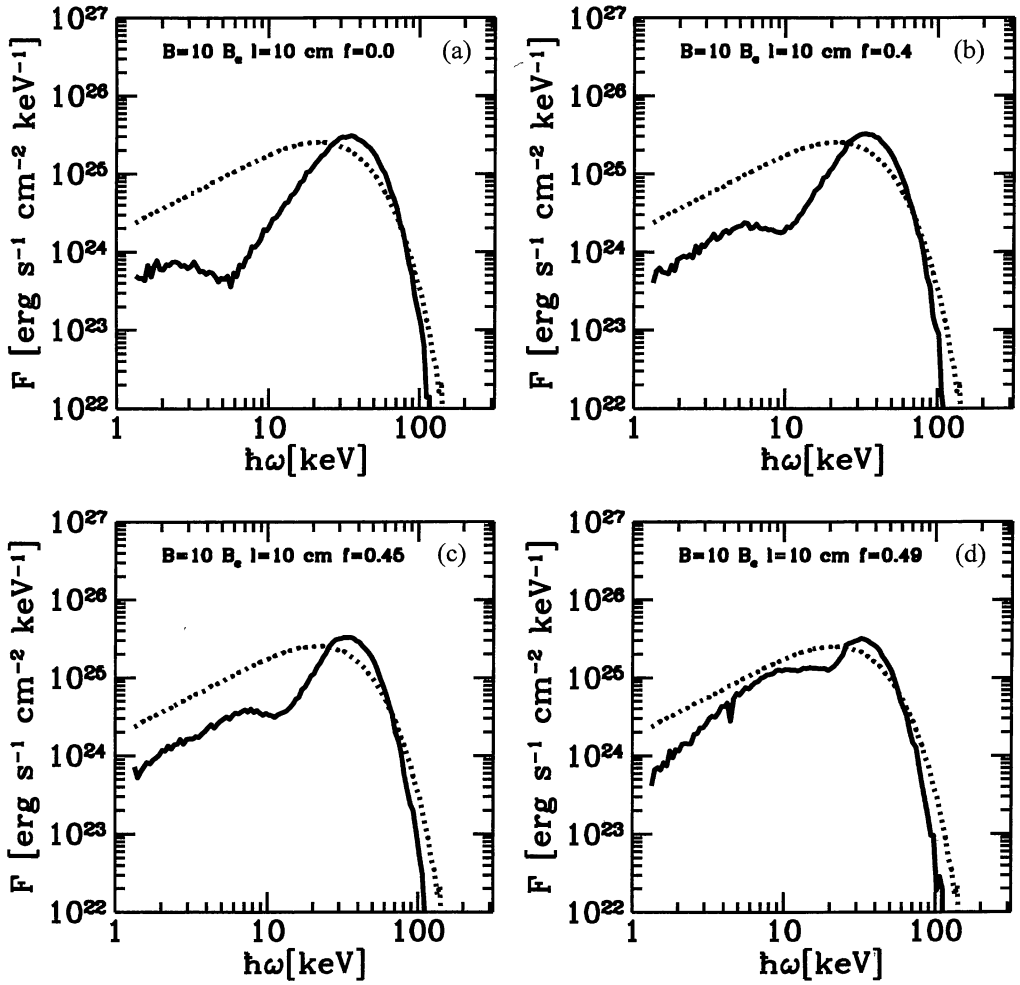

Figure 5. Model spectra, as seen at the stellar surface (solid lines), showing the effects of different pair densities. In each panel $B=10B_c$, $l=10$ cm, the input (dotted lines) is a 10-keV blackbody produced deep in the atmosphere, and the magnetic field is perpendicular to the surface. In panels (a), (b), (c) and (d), respectively, the pair fraction (defined as the ratio of the number of positrons to the total number of leptons) is $f=0$, 0.4, 0.45 and 0.49. As derived in Section 3, the pair fraction affects only the low-energy range of the vacuum feature.

and part comes from the angular dependences of scattering in a strong magnetic field. For a magnetic field in the surface, the emission also depends on azimuthal angle, but qualitatively the angle-dependent scattering and geometric effects partially cancel and the emergent radiation is closer to isotropic than if only geometric effects operated. We also note that, regardless of the orientation of the magnetic field, the photon energy spectrum is essentially independent of viewing angle.

5 DISCUSSION

Many of the spectra in the preceding section show prominent absorption-like features owing to the vacuum resonance. As discussed in Section 4.1, these features owe their existence in large part to the influence of Comptonization and mode switching, which imply that photons that interact in the resonance undergo frequency diffusion and spread their energy over the spectrum, creating a relative deficit at the original energy. In contrast, if Comptonization is neglected, the photons undergo primarily spatial diffusion, with minimal effects on the spectrum unless the atmosphere is of uniform density (see e.g. Ventura et al. 1979). Thus, in treatments of this effect that do not include Comptonization [such as the Bezchastnov et al. (1996) radiative transfer approach], the vacuum resonance will be smeared out by density gradients, whereas in our spectra the breadth and visibility of the absorption-like feature are partially *because* of the density gradients, as explained in Section 3.

In the preceding section we examined the vacuum resonance features produced for magnetic fields, scaleheights, and pair fractions like those expected in SGRs. We now summarize the qualitative effects of each parameter, and compare our theoretical spectra with the spectra seen in SGR 1806 – 20.

The physical quantity of greatest interest is the magnetic field, because above $\sim B_c$ many exotic processes play an important role. Our results show that, if a vacuum resonance feature is seen, the field must be stronger than $\sim B_c$. Since the location and strength of the feature depend only weakly on B, observation of the feature would only place a lower bound on the magnetic field; this would imply that the

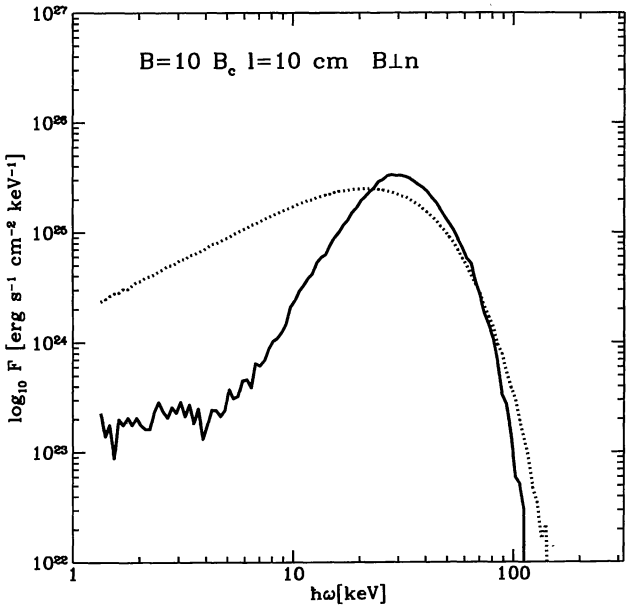

Figure 6. Model spectra, as seen at the stellar surface (solid line), for a magnetic field in the surface of the star. The input (dotted line) is a 10-keV blackbody. The low-energy spectrum is flatter than when the field is perpendicular to the surface.

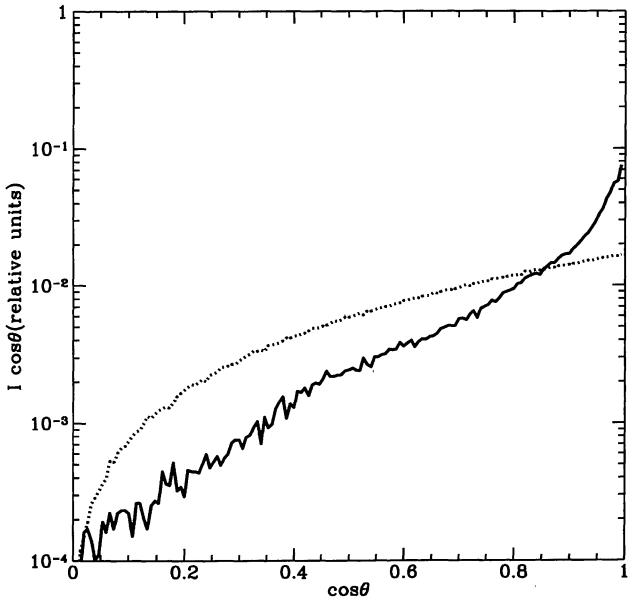

Figure 7. Angular distribution of emergent radiation (solid line) for a magnetic field perpendicular to the surface, showing a strong peak along the surface normal ($\mu=1$). For comparison, we also show a simulation of the angular distribution for isotropic scattering (dotted line).

field of the SGR was at least as strong as the strongest magnetic field inferred for a pulsar, 2×10^{13} G.

If the density structure of the atmosphere can be represented as exponential, then the scaleheight affects the qualitative nature of the observed spectrum. For large scaleheights $\ell\gtrsim1000$ cm, the feature is manifested as a drop-off at $\sim$40–50 keV, and the rise at lower frequencies is below 5 keV. If instead $\ell\lesssim10$ cm, both the low- and high-energy wings around the feature are in principle visible above 5 keV. These two regimes might be appropriate to a burst (for large scaleheights) and to afterglow (for small scaleheights). In particular, detailed time-resolved spectra whould show this transition as the luminosity drops.

The depth of energy production affects the lower bound to the vacuum resonance feature, and for a shallow enough production depth (say, 9 scaleheights when $B=10B_c$) the feature is not present. This implies that we may not expect to see such features in accretion-powered pulsars, even if their fields are very strong; typical stopping depths are $\lesssim50$ g cm^{-2} (Miller, Salpeter & Wasserman 1987), corresponding to less than 9 scaleheights.

The pair fraction f does not affect the location of the upper bound to the vacuum resonance feature, but does change the location of the lower bound. If the plasma density is dominated by pairs, the feature is narrowed and detectability requires that the source of photons be deeper than when the electron–baryon contribution dominates. If the magnetic field and scaleheight are known from other information, the centroid and width of the resonance feature would then tell us the pair density and the depth where photons were generated.

How do the spectra of the bursts from SGR 1806 – 20 fit into this picture? None of the spectra has obvious spectral features that clearly indicate a vacuum resonance. This is an indication (Fenimore et al. 1994) that there is a low-energy fall-off below $\sim$15 keV; this could be explained by a large scaleheight in our model, but many explanations not involving strong magnetic fields are equally viable. The *X-ray Timing Explorer*, with its large area (3000 cm^2 at 3 keV) and good spectral resolution (18 per cent at 6 keV), will, if it catches an SGR burst, give us much-needed spectral information in the range where features such as the vacuum resonance are expected to appear; the *High-Energy Transient Experiment* may likewise provide useful information, particularly with its Wide Field X-ray Monitor.

In conclusion, in magnetic fields $B\gtrsim B_c$ and plasma densities comparable to those expected in SGRs, photon scattering is strongly affected by the vacuum resonance. Since scattering opacity is likely to dominate over absorption opacity, this is an important effect which must be included in calculations of radiative transfer through strongly magnetized atmospheres.

ACKNOWLEDGMENTS

We thank Carlo Graziani, George Pavlov and Victor Bezchastnov for valuable discussions. This work was supported in part by NASA grant NAG 5-2868, and, through the *Compton* Fellowship Program, by NASA grant 5-2687.

REFERENCES

Adler S. L., 1971, Ann. Phys., 67, 599
Bezchastnov V. G., Pavlov G. G., Shibanov Yu. A., Zavlin V. E., 1996, in Kouveliotou C., Briggs M. F., Fishman G. J., eds, Proc. Third Huntsville Workshop on Gamma-Ray Bursts. Am. Inst. Phys., New York, p. 907
Chandrasekhar S., 1960, Radiative Transfer. Dover, New York
Evans W. D. et al., 1980, ApJ, 237, L7

Fenimore E. E., Laros J. G., Ulmer A., 1994, ApJ, 432, 742
Gnedin Yu. N., Pavlov G. G., Shibanov Yu. A., 1978, JETP Lett., 27, 305
Hurley K., Sommer M., Kouveliotou C., Fishman G., Meegan C., Cline T., Boer M., Niel M., 1994, ApJ, 431, L31
Katz J. I., 1982, ApJ, 260, 371
Katz J. I., 1993, in Friedlander M., Gehrels N., Macomb D. J., Compton Gamma-Ray Observatory. Am. Inst. Phys., New York, p. 1090
Katz J. I., 1994, ApJ, 422, 248
Kouveliotou C. et al., 1993, Nat, 362, 728
Kouveliotou C. et al., 1994, Nat, 368, 125
Kulkarni S. R., Frail D. A., 1993, Nat, 365, 33
Kulkarni S. R., Frail D. A., Kassim N. E., Murakami T., Vasisht G., 1994, Nat, 368, 129
Lamb D. Q., 1982, in Ligenfelter R. E., Hudson H. S., Worrall D. M., Gamma-Ray Transients and Related Astrophysical Phenomena. Am. Inst. Phys., New York, p. 249
Mazets E. P., Golenetskii S. V., 1981, Ap&SS, 75, 47
Mazets E. P., Golenetskii S. V., Ilyinskii V. N., Aptekar R. L., Guryan Y. A., 1979, Nat, 282, 587
Mészáros P., 1992, High-Energy Radiation from Magnetized Neutron Stars. Univ. Chicago Press, Chicago
Miller G. S., Salpeter E. E., Wasserman I., 1987, ApJ, 314, 215
Miller M. C., Bulik T., 1996, in Kouveliotou C., Briggs M. F., Fishman G., eds, Proc. Third Huntsville Workshop on Gamma-Ray Bursts. Am. Inst. Phys., New York, p. 956
Pavlov G. G., Gnedin Yu. N., 1984, Sov. Sci. Rev. E, 3, 197
Pavlov G. G., Shibanov Yu. A., 1979, JETP, 49, 74
Pavlov G. G., Shibanov Yu. A., Yakovlev D., 1980, Ap&SS, 73, 33
Thompson C., Duncan R. C., 1995, MNRAS, 275, 255
Tsai W., Erber T., 1974, Phys. Rev., D10, 492
Ventura J., Nagel W., Mészáros P., 1979, ApJ, 233, L125